Available online at www.sciencedirect.com

SCIENCE DIRECT®

Journal of Applied Geophysics 57 (2005) 129–153

JOURNAL OF APPLIED GEOPHYSICS

www.elsevier.com/locate/jappgeo

Evaluation of infiltration in layered pavements using surface GPR reflection techniques

K. Grote[a,*], S. Hubbard[b,1], J. Harvey[c,2], Y. Rubin[a,3]

[a]*Dept. of Geology, Univ. of Wisconsin-Eau Claire, 105 Garfield Ave., Eau Claire, WI 54702, USA*
[b]*Lawrence Berkeley National Laboratory, MS 90-1116, 1 Cyclotron Road, Berkeley, CA 94720, USA*
[c]*Civil and Environmental Engineering, Univ. of California, Davis, One Shields Avenue, Davis, CA 95616, USA*

Received 3 December 2003; accepted 26 October 2004

Abstract

The bearing capacity of sub-asphalt soils, which is a critical parameter for assessing pavement conditions and guiding pavement maintenance, is greatly influenced by soil water content. In this study, ground-coupled ground penetrating radar (GPR) techniques were used to non-destructively monitor the volumetric water content in sub-asphalt aggregate layers during an extended infiltration experiment. Water was injected over a period of several months into two differently layered pavement test sections, one of which contained a sub-asphalt drainage layer. GPR travel time data were used to estimate the water content in each aggregate layer and the variations in water content with time, and GPR amplitude data were used to indicate areas of high water content immediately beneath the asphalt layer. The GPR data revealed significant variations in the water content of the aggregate layers in both the horizontal and vertical directions and over time. Comparison of the water content estimates from GPR travel time data and from gravimetric water content measurements showed that the difference between the two techniques was approximately 0.02 cm^3/cm^3. These results suggest that GPR techniques can be used for accurate, non-invasive water content estimation in sub-asphalt aggregate layers and for assessing the efficacy of pavement drainage layers.

Keywords: Ground penetrating radar; Water content; Pavement aggregates; Reflection

1. Introduction

Accurately assessing the condition of existing pavements is essential for many transportation programs. In the United States, most pavement structures were constructed decades ago, and much of the current investment in pavements is in maintenance and rehabilitation (M&R) rather than in new construction. The type and extent of M&R are partially

* Corresponding author. Tel.: +1 715 836 5485; fax: +1 715 836 5627.
E-mail addresses: grotekr@uwec.edu (K. Grote), sshubbard@lbl.gov (S. Hubbard), jtharvey@ucdavis.edu (J. Harvey), rubin@ce.berkeley.edu (Y. Rubin).
[1] Tel.: +1 510 486 5266; fax: +1 510 486 5686.
[2] Tel.: +1 530 754 6409; fax: +1 530 752 7872.
[3] Tel.: +1 510 642 2282; fax: +1 510 642 7476.

0926-9851/$ - see front matter © 2004 Elsevier B.V. All rights reserved.
doi:10.1016/j.jappgeo.2004.10.002

based upon the assessed bearing capacity of the sub-asphalt soils, where the bearing capacity is defined as the ability to carry a defined number of repetitions of a set of loads. If the bearing capacity of the sub-asphalt soils is not assessed correctly, the estimated M&R requirements may be inaccurate, and the M&R design may be either overly conservative or inadequate. Currently, falling weight deflectometers (FWDs) are the most commonly used method for estimating pavement bearing capacity, where the bearing capacity is determined by measuring deflections that reflect the pavement stiffness. The pavement bearing capacity is a function of the bearing capacity of the sub-asphalt soil, which is greatly affected by the soil water content (Hicks, 1970; Fang, 1991) and soil suction (Heath, 2002). Increases in the water content of the sub-asphalt soils can decrease the soil stiffness and cause greater pavement deflections (Scullion et al., 1995; Kelley, 1999). Pavement stiffness estimates obtained with FWDs provide single measurements of a cyclic phenomenon and must be adjusted for moisture conditions that differ from the conditions at the time of the FWD survey. Ground penetrating radar (GPR) methods have the potential to estimate the water content in sub-asphalt soils coincidently with the FWD measurements. These in-situ, field-scale water content estimates could be used in conjunction with conventional laboratory relationships between water content and soil stiffness and strength to more accurately estimate the pavement bearing capacity under fluctuating moisture conditions. GPR methods could also be used during or immediately after wetter periods to determine the maximum likely water content of the sub-asphalt soil, which could be used to estimate the lowest probable pavement stiffness.

The water content in sub-asphalt aggregate soils can also be used to guide M&R of the overlying asphalt layer. Researchers have shown that moisture within the asphalt layer and the underlying soil can cause the bond between the asphalt cement and pavement aggregates to fail, resulting in asphalt 'stripping', which greatly decreases the service life of the asphalt layer (Scullion et al., 1994; Maser, 1996). GPR data could be used to non-invasively indicate areas of high water content beneath the asphalt layer to predict where erosion of the low-permeability interface between the asphalt layer and the aggregate soils and subsequent infiltration of water into the asphalt layer is most likely.

Estimates of the water content in sub-asphalt soils are also necessary to determine the efficacy of pavement drainage systems and to evaluate the need for drainage in undrained pavements. The costs of installing and maintaining sub-asphalt drainage systems are substantial. However, the design of drainage systems and the selection of pavements to be retrofitted with a drainage system are often made with little information regarding water contents in the sub-asphalt soil layers. As a result, expensive drainage systems may be installed in pavements where they offer only marginal benefits, or drainage systems may be omitted in some areas where they would greatly extend the service life of the pavement. GPR techniques could be used to obtain sub-asphalt water content estimates that would allow more efficient design and allocation of drainage systems.

Current techniques for estimating sub-asphalt water content include gravimetric sampling, time domain reflectometry (TDR), neutron probe logging and capacitance or resistance devices. These methods are invasive, expensive and time-consuming, and they may have high errors due to the water-cooled drill bits generally used for installation or sampling. Additionally, because soil water content is spatially variable, these point measurement techniques are of limited value when assessing the water content over large areas. For these reasons, sub-asphalt water contents are not estimated for most pavement applications. GPR techniques are non-destructive and can be collected quickly over large areas, and are therefore potentially more suitable than conventional methods for water content estimation in pavements.

Researchers and engineers have used GPR techniques for a variety of pavement applications, such as measuring pavement thickness (Cuvillier et al., 1987; Eckrose, 1989; Fernando and Maser, 1991; Roddis et al., 1992), detecting voids beneath pavements (Clemena et al., 1986; Bomar et al., 1988; Smith and Scullion, 1993; Saarenketo and Scullion, 1994), evaluating bridge decks (Clemena, 1983; Maser, 1991; Maser and Rawson, 1992) and estimating rebar corrosion (Narayanan et al., 1998; Hubbard et al., 2003). GPR data have also been used for water content estimation in pavement materials; Saarenketo

et al. (1994) used GPR amplitude data to qualitatively monitor the infiltration of saline water injected alongside a highway; and Scullion et al. (1995) used GPR amplitude data to quantitatively estimate water content in pavement aggregates for four controlled laboratory samples. Additionally, several researchers have used GPR travel time data for quantitative water content estimation for other applications. Very near-surface (uppermost 20 cm) soil water content estimates have been calculated in field-scale experiments using GPR groundwave travel time data (Du and Rummel, 1994; Lesmes et al., 1999; Hubbard et al., 2002; Grote et al., 2003), and deeper estimates of water content have been calculated in soil layers using GPR reflection travel time data (Greaves et al., 1996; Van Overmeeren et al., 1997; Weiler et al., 1998; Grote et al., 2002; Lunt et al.,). This study extends the previous results by utilizing common-offset GPR travel time data in a field-scale experiment to quantitatively estimate sub-asphalt water content under engineered conditions.

In this study, GPR techniques were used to estimate the sub-asphalt water content in pavement aggregate soils for two differently layered pavement sections during a period of prolonged infiltration. GPR travel time data were used to estimate the water content in each aggregate layer, and GPR amplitude data were used to indicate areas of high water content immediately beneath the asphalt layer. A brief background of the GPR techniques used in this study is given in Section 2, and Section 3 describes the experimental procedures. In Section 4, the results of the travel time and amplitude analyses for both pavement sections are discussed, and the water content estimates from GPR travel time data and gravimetric measurements are compared. The conclusions from this experiment and the subsequent implications for GPR pavement applications are given in Section 5.

2. GPR background

GPR is a high frequency electromagnetic technique that emits a signal of fixed voltage and frequency and records the subsurface response as a time series of voltages (amplitude). The electromagnetic property most commonly measured using GPR data is the dielectric constant (κ), which for typical operating frequencies and surveying environments is primarily influenced by the soil water content (Davis and Annan, 1977; Topp et al., 1980). Both the travel time and amplitude of the GPR signal can be used to estimate the dielectric constant if the subsurface material has low electrical conductivity and the GPR data are acquired using standard high frequency (~50–1500 MHz) antennas. Travel time measurements from GPR reflections can be used to determine the electromagnetic velocity (v) to an interface, and the velocity can then be used to estimate the dielectric constant (κ):

$$\kappa \approx \left(\frac{c}{v}\right)^2, \tag{1}$$

where c is the plane-wave propagation velocity of electromagnetic waves in free space (Davis and Annan, 1989). Travel time measurements are most effective for estimating the dielectric constant when the subsurface geometry is known or when variable-offset data are acquired.

Amplitude data from GPR reflections may also be used to estimate the dielectric constant in many surveying environments. The amplitude of the received GPR signal is a function of the strength of the transmitted signal, the coupling between the GPR antennas and the ground, the travel path of the signal, the electromagnetic attenuation (α) of the subsurface materials and the interfaces encountered by the signal. The amplitude decreases with longer travel paths and higher attenuation, and the GPR signal may not be detectable for even very short travel paths in environments with very high attenuation. Electromagnetic attenuation is a function of the electrical conductivity (σ) of the subsurface materials and the frequency of the GPR transmitter, where attenuation is greater in environments with higher electrical conductivity and when higher frequency GPR antennas are employed. Attenuation in air, which has a very low electrical conductivity, is usually considered negligible for most frequencies. For environments with low electromagnetic attenuation, the dielectric constant can be estimated from measurements of GPR attenuation and the electrical conductivity (Davis and Annan, 1989):

$$\sqrt{\kappa} \approx \frac{1.69 \times 10^3 \sigma}{\alpha}. \tag{2}$$

However, attenuation estimates are very difficult to quantitatively extract from most surface-based GPR data, the approximation given in Eq. (2) is not appropriate for all surveying environments, and the electrical conductivity of subsurface materials is usually unknown. Thus, estimation of the dielectric constant using surface-based GPR attenuation data is very challenging.

A more practical application of GPR amplitude data is to analyze the amplitudes of reflections to determine information about the dielectric constant on either side of the reflective interface. The reflection amplitude indicates the proportion of energy that is reflected from an interface or transmitted into the next layer; high amplitude reflections indicate a large contrast in dielectric constant between layers. For example, a wet layer (with a high dielectric constant) underlying a dry layer (low dielectric constant) would generate a high amplitude reflection, whereas two layers with very similar water contents would generate a low amplitude reflection. The amplitude reflection coefficient (RC) can be used to quantify the proportion of reflected energy at an interface as a function of the dielectric constants of the layers above (κ_1) and below (κ_2) the interface (Ulriksen, 1992):

$$RC = \frac{\sqrt{\kappa_1} - \sqrt{\kappa_2}}{\sqrt{\kappa_1} + \sqrt{\kappa_2}}. \quad (3)$$

To use the reflection coefficient to estimate the dielectric constant of an underlying layer, it is first necessary to determine the dielectric constant of the overlying layer. For air-launched GPR data, the dielectric constant of the overlying material (air) is known (κ_{air}=1). Thus, the amplitude of the reflection from the air-ground interface can be used to determine the dielectric constant of the surficial material, after the amplitude of the air-ground reflection has been calibrated by the amplitude of a reflection from a large metal plate (Saarenketo and Scullion, 2000). After the dielectric constant of the surficial material has been calculated, the dielectric constant of underlying layers can be estimated using the reflection amplitudes from deeper interfaces. However, the equations commonly used to approximate the dielectric constant from reflection amplitudes do not account for attenuation of the GPR signal with increased propagation distance. This omission does not significantly affect the accuracy of the dielectric constant estimated from the initial air-ground reflection, because the attenuation of electromagnetic energy in air is usually low. However, attenuation in subsurface materials is often significant. For pavement applications, attenuation of the GPR signal in concrete and aggregate layers is typically considerable and may reduce the accuracy of dielectric constant estimates from amplitude data for deeper subsurface layers (Saarenketo and Scullion, 2000).

For many pavement applications, the dielectric constant has been estimated using amplitude analysis of common-offset air-launched GPR data (Cuvillier et al., 1987; Fernando and Maser, 1991; Roddis et al., 1992; Scullion et al., 1995), where common-offset data are acquired by keeping the transmitting and receiving antennas a constant distance apart and pulling them in parallel along a traverse. Air-launched data can be collected very quickly (at highway speeds) and can be used to easily determine the dielectric constant of the surficial layer without reflections from deeper layers. However, the penetration depth of air-launched data is usually small (from 0.5 to 0.9 m) (Saarenketo and Scullion, 2000). Air-launched data have a limited penetration depth because the energy emitted from a GPR dipole antenna in a uniform media (such as an antenna suspended in air) radiates outwards both laterally and vertically (so less energy is directed into the ground), energy is lost due to spherical spreading of the signal in air, and energy is reflected from the air-ground interface rather than penetrating into the ground.

To provide more accurate estimates of the dielectric constant for deeper pavement layers, ground-coupled GPR travel time data can be employed. Ground-coupled data can have penetration depths as deep as 50 m in clean natural sediments (Davis and Annan, 1989). Although penetration depths of this magnitude are not expected for materials common to transportation applications, ground-coupled GPR methods can probe the entire pavement structure. Ground-coupled amplitude data cannot be used to quantitatively estimate the dielectric constant in pavement aggregates using the reflection coefficient approach described by Eq. (3), as ground-coupled data do not allow for calibration with a metal plate and the dielectric constant of the uppermost layer is not

known. However, travel time measurements from the ground-coupled data can be used to estimate the dielectric constant, and these estimates are not subject to errors due to amplitude attenuation. Thus, ground-coupled travel time data offer an approach for accurately estimating the dielectric constant in sub-asphalt aggregates, which can be subsequently used to estimate the water content and soil stiffness and strength or to assess drainage layer efficacy. Additionally, although the ground-coupled amplitude data cannot be used quantitatively to estimate water content, reflection amplitudes from ground-coupled data can be qualitatively analyzed to indicate the degree of contrast between the dielectric constants of different layers.

After the dielectric constant has been estimated from either travel time or amplitude data, numerous relationships are available to correlate this value to volumetric water content. Empirical relationships, such as the equation developed by Topp et al. (1980) using a range of soil types, or volumetric mixing models (Alharthi and Lange, 1987; Roth et al., 1990) can be employed for converting dielectric constant to water content. For increased accuracy, site-specific petrophysical relationships can also be developed using soil samples and TDR techniques.

3. Experimental approach

In this study, we tested the accuracy and resolution of ground-coupled GPR travel time data for estimating the water content in drained and undrained pavement aggregates. Section 3.1 describes the experimental pavements and infiltration system used in this study, while the data collection, processing and interpretation techniques are discussed in Section 3.2. The petrophysical relationships used to convert the travel time measurements to water content estimates are also given in Section 3.2.

3.1. Experimental configuration

This experiment was performed in a large metal shed (9×100 m), within which two differently layered pavement sections (drained and undrained) were constructed on the natural clay subgrade. The design for both pavement sections followed typical California Department of Transportation (Caltrans) specifications, and the methods used to create the pavements were those commonly used in Caltrans construction. Each pavement had 3.8 cm of asphalt rubber overlay and 13.2 cm of asphalt concrete (AC) overlying the aggregate layers. In the drained pavement section, the asphalt was underlain by a nearly uniformly graded layer of coarse gravel mixed with a very small percentage (about 5% by volume) of asphalt. This material is the asphalt treated permeable base (ATPB), which has a porosity of around 30% and serves as the drainage layer for the pavement. Beneath the ATPB in the drained section and beneath the AC in the undrained section is the aggregate base (AB), which is composed of a densely graded, medium to coarse gravel compacted to approximately 100% density relative to modified Proctor. The high degree of compaction applied to the AB gives this layer a relatively low permeability. The surface of the AB was sprayed with a penetrating film of oil and asphalt (prime coat) prior to placement of the ATPB and AC in the drained and undrained pavements, respectively. Underlying the AB for both sections is the aggregate sub-base (ASB), which is similar to the AB in composition, but has a slightly higher percentage of fines and is

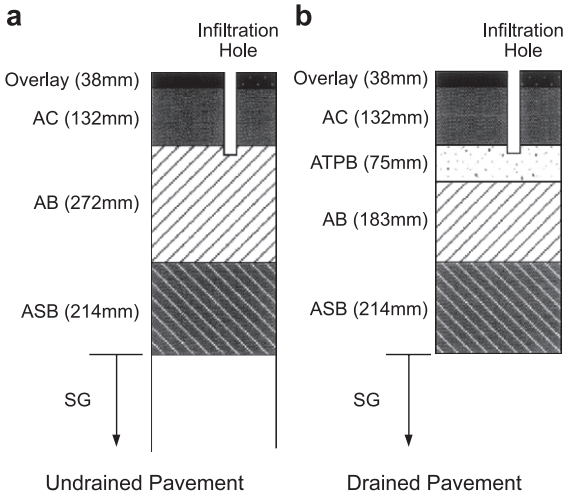

Fig. 1. Vertical cross-section of the experimental pavements illustrating the thickness of the rubber overlay, AC, AB, ASB and SG. (a) Undrained pavement and (b) drained pavement.

not as heavily compacted. Permeability tests have shown the ASB to be significantly more permeable than the AB. The ASB is the lowermost engineered layer; beneath it is the subgrade (SG), which at this site is a highly plastic deltaic clay compacted to approximately 95% density relative to modified Proctor to a depth of 15 cm. A cross-section of both pavements is shown in Fig. 1. The pavement layers have a primary gradient of 2–3% and a perpendicular secondary gradient of 0.5% across each section.

Water was introduced into the uppermost aggregate layer of both pavement sections by means of a drip infiltration system. The infiltration system consisted of a series of 2.5 cm diameter holes drilled through the AC and through the top 2.5 cm of the ATPB (drained pavement) or AB (undrained pavement) at 0.5-m intervals along a 12-m length on the upgradient side of each pavement section. A drip hose attached to a main pump and timing system was inserted into each hole, and a nozzle at the end of each drip hose regulated the rate of infiltration. The locations of the infiltration holes for both pavement sections are shown in Fig. 2a and b. Since both pavement sections were located inside a building, changes in the water content of the aggregate layers were expected to occur only as a result of the introduced infiltration; the effects of outside precipitation were expected to be negligible. This infiltration scheme simulated surface water

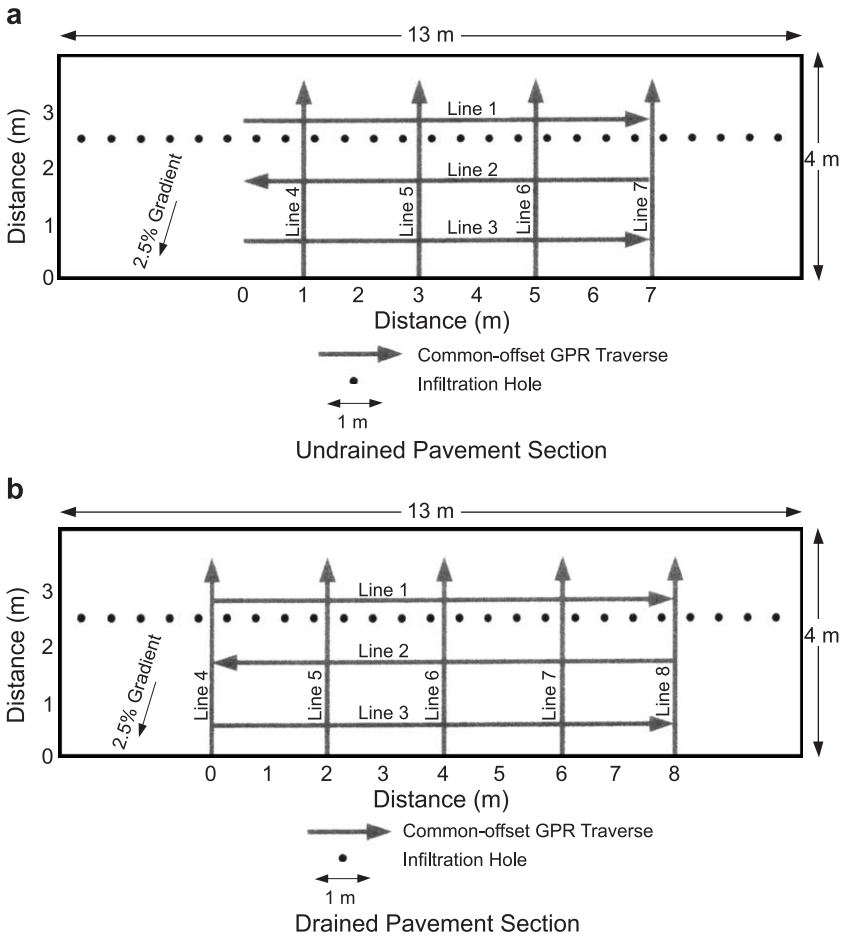

Fig. 2. Map view of the experimental pavement sections showing the locations of the infiltration holes and the GPR traverses. (a) Undrained pavement section and (b) drained pavement section.

entering through a cracked AC layer in damaged pavements.

3.2. Experimental procedures

3.2.1. Data collection

GPR data were collected at two frequencies (900 and 1200 MHz) using a ground-coupled Sensors and Software's PulseEkko1000 surface GPR system. The frequency bandwidth was approximately equal to the central frequency, and the antenna separation was 17 and 7.5 cm for the 900- and 1200-MHz data, respectively. An odometer was used to trigger data collection at 2-cm intervals, and data were stacked 16 times at each station to improve the signal to noise ratio. For each pavement section, a grid of GPR data was collected along the traverses shown in Fig. 2.

Different rates of infiltration were used for each pavement section, and the time intervals between GPR surveys varied correspondingly. For the drained pavement, three rates of infiltration were used to simulate light, medium and heavy rainfall as defined by precipitation records in northern California, and several GPR surveys were collected during each infiltration rate. The lowest infiltration rate (98 l/day) was applied initially, and it was continued for 2 weeks before increasing the infiltration rate to 151 l/day. This infiltration rate was also applied for 2 weeks, then was increased to the highest rate of 233 l/day. Infiltration was applied at the highest rate for approximately 5 weeks. For each rate, infiltration occurred every 6 h, with the duration of infiltration and the volume of water released into each hole calculated to achieve the desired l/day rate across the 12-m infiltration zone. For the undrained pavement section, a similar infiltration and data collection procedure was followed, but only one infiltration rate (11 l/day over the 12-m injection zone) was used. This low infiltration rate was chosen because higher rates resulted in persistent overflowing of the infiltration holes. Infiltration was continued at this rate for approximately 33 weeks, and GPR data were collected periodically throughout this time. GPR data were collected less frequently in the undrained pavement than in the drained pavement due to the very low rate of infiltration and the expectation of gradual change in the water content of the undrained pavement aggregates.

3.2.2. Data processing and interpretation

The processing routine applied to the GPR data was simple, although more sophisticated data processing techniques were initially investigated. The final data processing routine included a low-cut filter to remove induction effects, a very mildly time-varying bandpass filter designed to retain the dominant frequencies observed in the data, trace-averaging over the number of measurements in the radar 'footprint' and automatic gain control (AGC). The AGC was necessary to detect the reflection from the deepest interface in the 1200-MHz data, but also increased the amplitude of the noise in the shallower data.

Interpretation of the GPR data involved analyzing and comparing the reflections observed in 900-MHz common-midpoint (CMP) data with common-offset data from both frequencies. The antenna housing of the 1200-MHz antennas did not allow separation of the transmitting and receiving antennas, so 1200-MHz CMP data could not be collected, but the 900-MHz antennas were separable. The 900-MHz CMP data were used to identify the reflections from aggregate layer interfaces, and the arrival times of these reflections were used to interpret both the 900- and 1200-MHz common-offset data. The 1200-MHz data had very high resolution and showed reflections from the main interfaces between the asphalt concrete and aggregate layers, but also revealed multiples from the asphalt concrete-aggregate interface and reflections from layers (lifts) within the aggregate layers. (The aggregate layers were constructed in lifts ~11 cm thick, and the soil was compacted after placement of each lift. This construction method causes the soil density to be greater near the top of a lift than at the bottom, and if the change in soil density is significant, a GPR reflection can be generated from the lift boundaries.) To determine which reflections corresponded to major interfaces between aggregate layers, the 1200-MHz data were compared to the 900-MHz data. The 900-MHz data have lower resolution but better penetration, and these data more clearly showed reflections from major interfaces without as many minor reflections from lifts between the layers.

An example of the 900- and 1200-MHz data collected over the undrained pavement section is shown in Fig. 3. Fig. 3a shows a 900-MHz CMP on which the airwave, groundwave and reflections from aggregate layers are identified, while Fig. 3b shows a 900-MHz common-offset traverse collected near the CMP. For both of these surveys, the reflection 'picks' were chosen as the first lobe of the Ricker

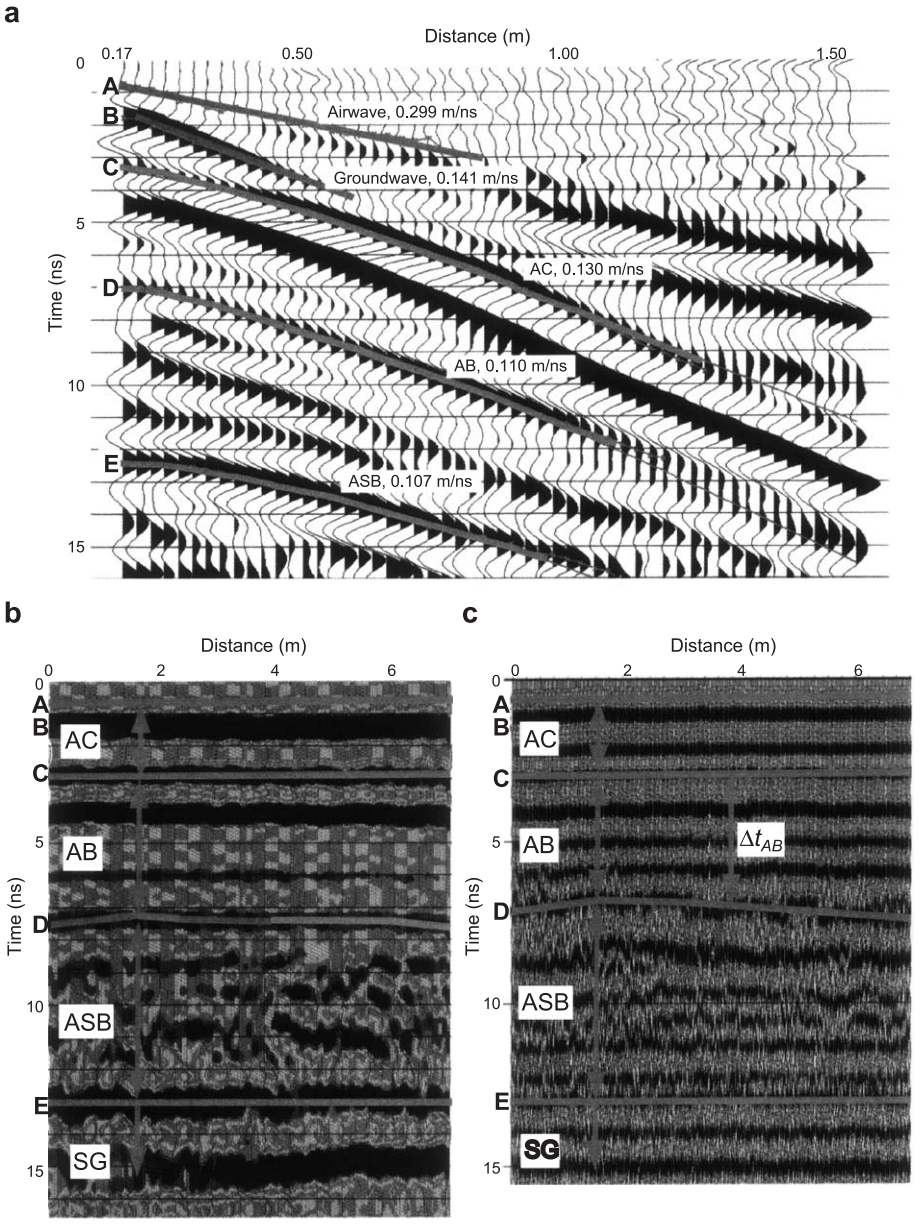

Fig. 3. Interpreted GPR data collected over the undrained pavement prior to infiltration. (a) 900-MHz CMP survey collected near the center of the section. (b) 900-MHz common-offset traverse collected along line 2 (Fig. 2a). (c) 1200-MHz common-offset traverse collected along line 2 (Fig. 2a).

wavelet for each reflection to reduce errors caused by dispersion of the wavelet. Using the first wavelet lobe to identify a reflector causes the reflection 'pick' to have the opposite polarity of the highest amplitude (central) lobe of the wavelet. For the GPR system employed in this study, the emitted GPR signal is a Ricker wavelet starting with a low-amplitude negative lobe, followed by a high-amplitude positive lobe, and ending with another low-amplitude negative lobe. For reflections with positive reflection coefficients (signal travels from a wetter soil to a drier soil), the reflected wavelet has the same polarity as the emitted wavelet, while negative reflection coefficients will result in a reflection wavelet of the opposite polarity. In the undrained pavement, the first reflection is from the AC–AB interface, which has a negative reflection coefficient. In Fig. 3a and b, this reflection can be seen as a high-amplitude trough (negative amplitude, shown in white) flanked by two lower-amplitude peaks (positive amplitude, shown in black). Following our picking convention, the reflection 'pick' is chosen as the lower-amplitude peak preceding the high-amplitude trough. The reflection picks from the AB–ASB and ASB–SG interface were similarly chosen. The airwave, used to determine the 'zero time', was chosen as the low-amplitude trough preceding the main airwave peak. As can be seen in the 900-MHz CMP (Fig. 3a), the main airwave peak is partially superimposed with the groundwave at small antenna offsets, so the convention of picking the first lobe of each wavelet also helps to reduce the effects of superposition at these offsets. Fig. 3c shows a common-offset 1200-MHz traverse collected immediately after the 900-MHZ data. The arrival times of major reflections in the 900- and 1200-MHz data matched fairly well, although some minor discrepancies were observed. Small differences between the arrival times of 900- and 1200-MHz reflections are partially due to the different antenna separations of each frequency, which create a slightly longer travel path for the 900-MHz data. Slight variations in the arrival times might also be caused by differences in bandwidth for the two frequencies, which result in different resolutions.

Examples of 900- and 1200-MHz data collected over the drained pavement are shown in Fig. 4. This figure shows the reflections between aggregate layers, where the same procedures for identifying and 'picking' reflections were used as for the undrained pavement. Fig. 4a (900-MHz CMP) and Fig. 4b (900-MHz common-offset traverse collected near the CMP) show that no clear reflection was generated from the ATPB in the 900-MHz data, as the resolution of the 900-MHz data was too low to detect this thin layer. In the 1200-MHz data, a fairly low-amplitude reflection that had the expected polarity and arrival time was identified as the AC–ATPB interface, but this identification was not verified through CMP analysis given the limitations of the 1200 MHz antennas. The deeper reflections in the drained pavement have similar arrival times for the 900- and 1200-MHz data.

After the primary reflectors in the common-offset data had been identified by comparison with CMP data, the average electromagnetic velocity in each layer (estimated from CMP velocity analysis) was used in conjunction with the known thickness of each layer to estimate the approximate travel time through the layer. The validity of the common-offset interpretation was then verified by determining that the measured travel time between common-offset reflections was similar to the estimated travel time. Common-offset reflections were also inspected to verify that the primary reflections did not appear to be multiples of earlier reflections and that sufficient variation in travel time was observed for each reflector to indicate that the reflection imaged a subsurface interface and was not system noise. The common-offset traverses shown in Figs. 3 and 4 were collected along line 2 (Fig. 2a and b) before the start of infiltration, and the water content was assumed to be fairly uniform throughout both pavement sections at this time. The variations in travel time observed in some of the aggregate layers in Figs. 3 and 4 suggest that the thicknesses of the aggregate layers were not perfectly uniform across each section.

3.2.3. Travel time calculations

The travel time of the electromagnetic energy through each layer was calculated as the difference in arrival times of the reflections from layer interfaces. For example, the two-way travel time through the AB in the 1200-MHz data is indicated as Δt_{AB} in Figs. 3c and 4c. After the travel time through each layer was

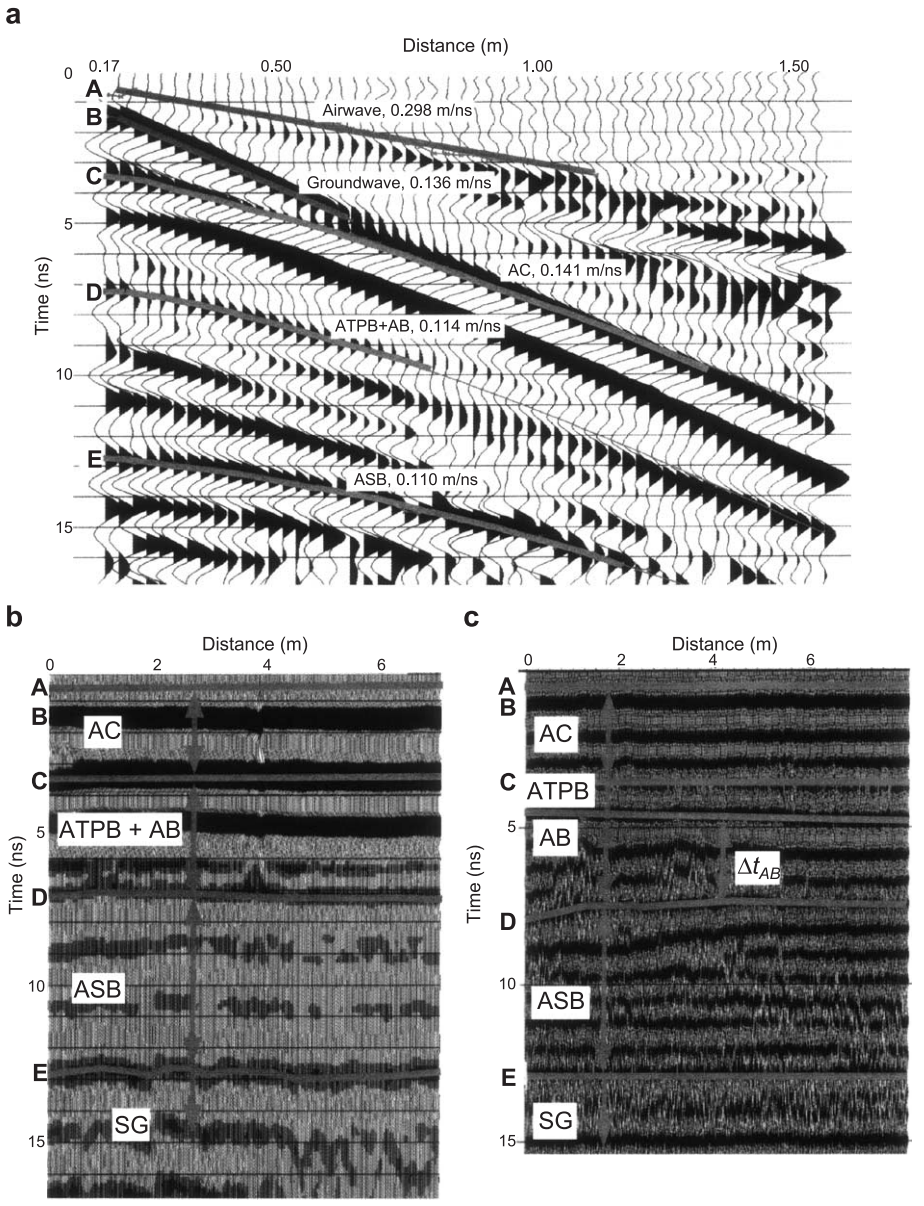

Fig. 4. Interpreted GPR data collected over the drained pavement prior to infiltration. (a) 900-MHz CMP survey collected near the center of the section. (b) 900-MHz common-offset traverse collected along line 2 (Fig. 2b). (c) 1200-MHz common-offset traverse collected along line 2 (Fig. 2b).

calculated, the electromagnetic velocity (v) at each point was estimated using the two-way travel time and the known average thickness (d) of each layer:

$$v = \frac{2d}{\Delta t}. \tag{4}$$

The velocity was then converted to dielectric constant using Eq. (1), and the volumetric water content was estimated from the dielectric constant using petrophysical relationships. Site-specific petrophysical relationships were developed in the laboratory for the AB and ASB using TDR techniques and samples

of the aggregate soils at different water contents (William Herkelrath, USGS, pers. comm.). The site-specific relationship for the AB was:

$$\theta_v = -1.98 \times 10^{-5}\kappa^3 + 2.39 \times 10^{-4}\kappa^2 + 1.95 \times 10^{-2}\kappa - 2.08 \times 10^{-2}, \quad (5)$$

where θ_v is the volumetric water content and κ is the bulk dielectric constant of the soil sample. Similarly, the site-specific relationship for the ASB was:

$$\theta_v = -1.04 \times 10^{-6}\kappa^3 + 2.47 \times 10^{-4}\kappa^2 + 2.45 \times 10^{-2}\kappa - 4.52 \times 10^{-2}. \quad (6)$$

A site-specific relationship could not be developed for the ATPB, as the asphalt cement caused this layer to be impenetrable to TDR probes. Instead, Topp's equation:

$$\theta_v = 4.3 \times 10^{-6}\kappa^3 - 5.5 \times 10^{-4}\kappa^2 + 2.92 \times 10^{-2}\kappa - 5.3 \times 10^{-2} \quad (7)$$

(Topp et al., 1980) was used for estimating water content from the dielectric constant measurements within the ATPB. Topp's equation is not entirely appropriate for water content estimation in this layer, as this relationship was developed on soils with fairly uniform water content distributions, and the water content distribution in the ATPB tends to be quite irregular, as will be discussed later. Thus, water content estimates in the ATPB obtained with Topp's equation are more appropriate for assessing the relative moisture conditions in the ATPB compared to dry conditions than for accurately quantifying the water content.

To most accurately estimate the sub-asphalt water content from GPR data, precise travel time measurements across each aggregate layer are needed. Higher frequency GPR data have better resolution, and thus more accurate travel time measurements, than lower frequency data. The travel time measurements through the aggregate layers were therefore calculated using the highest frequency (1200-MHz) data whenever feasible. However, the 1200-MHz data did not always provide consistent reflections from the lowermost interface (ASB–SG reflection), so the 900-MHz data were also employed for some of the travel time measurements, as is discussed below.

Although the surveys collected prior to infiltration showed clear reflections from each layer interface, some of these reflections were more difficult to identify reliably in the 1200-MHz data for the surveys collected more than a few weeks after the start of infiltration. Specifically, the amplitudes of the reflection from the ASB–SG interface decreased significantly in later surveys, until this interface was difficult to pick consistently using 1200 MHz data. The reduced amplitudes of this reflection probably result from increased attenuation of the high-frequency electromagnetic energy in the overlying aggregate layers as the water content of these layers increased, but may also indicate a smaller reflection coefficient for the ASB–SG interface as the difference between the water contents of the ASB and the SG decreased. Attenuation is greatest at high frequencies, so the 1200-MHz data were more attenuated than the 900-MHz data, and the reflection from the ASB–SG interface could be measured easily in the 900-MHz data for all surveys. Therefore, the travel time through the ASB was calculated by subtracting the travel time between the airwave arrival (used to indicate the 'zero time') and the AB–ASB reflection in each 1200-MHz trace from the travel time between the airwave and the ASB–SG reflection in each 900-MHz trace for all points in each survey.

Another reflection that became more difficult to pick reliably with increased time after infiltration was the reflection from the AC–ATPB interface. This reflection occasionally had low amplitude or reversed polarity signals for the surveys collected several weeks after the start of infiltration. The changes in the amplitude of this reflection may be indicative of stripping in the AC or the ATPB; previous researchers have shown that asphalt stripping can result in polarity reversals of the reflected signal and that moisture in the asphalt can also alter the reflected waveform (Scullion et al., 1995; Scullion and Rmeili, 1997). Another possible reason for the changes in amplitude of this reflection is that water may be pooling on the low-permeability asphalt layer at the bottom of the ATPB, and this pooled water may cause a very large contrast in dielectric constant along the ATPB–AB interface. A reflection from pooled water would have very high amplitudes and could partially superimpose with (and destructively interfere with) the low amplitude reflection from the AC–ATPB interface,

which was easily detectable during the earlier surveys. To circumvent the changes in amplitude and polarity that made the AC–ATPB reflection difficult to pick for some surveys, the initial survey (collected before the start of infiltration) was used to define the travel time through the AC at all points for all subsequent surveys. As shown in Fig. 1, the infiltration holes extended through the AC into the first aggregate layer, so we do not anticipate changes in the water content of the AC, and thus the travel time through the AC can be assumed to be constant for all surveys. The travel time through the ATPB was calculated by subtracting, for each point in the survey grid, the travel time through the AC during the initial survey from the travel time through the AC plus the ATPB for each of the surveys collected during infiltration. This procedure allowed estimation of the travel time through the ATPB even when the AC–ATPB interface was difficult to pick, but increases the uncertainty of the water content estimates in this layer.

3.2.4. Amplitude calculations

In addition to using GPR travel time data to quantitatively estimate water content in the sub-asphalt aggregate layers, amplitude data from the reflection of the AC–aggregate interface were also used to indicate wetter or dryer areas immediately beneath the AC. The water content along the AC–aggregate interface could be significant for detecting stripping and subsequent deterioration of the AC. As the amplitudes from the ground-coupled GPR data could not be used to quantitatively determine the reflection coefficient of the AC–aggregate interface (due to attenuation of the signal in the AC and the absence of an air-surface reflection, as described in Section 2), the dielectric constant of the uppermost aggregate layer could not be estimated from the amplitude data. However, the reflection amplitudes could be used to indicate the degree of contrast in dielectric constant between the AC and the underlying aggregate layer, as described by Eq. (3). An increase in the water content of the aggregate layer would increase the dielectric constant of this layer, and thus would increase the contrast with the dielectric constant of the AC, which is assumed to be unchanging. The amplitudes of the AC–aggregate reflection therefore indicate the relative water content of the upper portion of the aggregate layer, where higher amplitudes correspond to wetter zones. For this study, the amplitude of the reflection from the AC–aggregate interface in the 1200-MHz data was normalized by the amplitude of the airwave for each trace to reduce any effects from voltage fluctuations in the GPR equipment for different surveys. The amplitude data were generated by arithmetically averaging the absolute values of the amplitudes within a window 0.5-ns wide centered on the reflection from the AC–ATPB interface in the drained pavement and from the AC–AB interface in the undrained pavement. A similar averaging procedure was performed for the airwave prior to normalizing the reflection from the AC–aggregate interface.

4. Experimental results and discussion

GPR travel time and amplitude data were analyzed for the surveys collected over both experimental pavements. Sections 4.1 and 4.2 discuss the results of these analyses for the undrained and drained pavements, respectively. After infiltration and monitoring of the experimental pavements were completed, gravimetric water content measurements were collected in both pavement sections and were compared to the GPR-derived water content estimates, as will be described in Section 4.3.

4.1. Results in the undrained pavement

In the undrained pavement, infiltration occurred into the upper portion of the AB, as shown in Fig. 1a, and GPR data were collected along the grid shown in Fig. 2a. GPR travel time measurements (such as those shown in Fig. 3c) were used to estimate the water content in the AB and ASB; the results of these travel time analyses are described in Section 4.1.1. GPR amplitude data were used to indicate wetter areas in the upper portions of the AB, as will be discussed in Section 4.1.2.

4.1.1. Water content estimates from GPR travel time data

Water content estimates in the AB and ASB were generated from GPR travel time data for each survey. To illustrate how water content varied with time, and to evaluate the horizontal water content distribution

independently of variations in pavement thickness, the changes in water content (compared to the 'dry' survey collected before infiltration began) were calculated, where the difference between the water content of a survey collected during infiltration and the water content of the 'dry' survey was calculated for each point in the GPR grid. Fig. 5 shows the average change in water content per survey for the AB and the ASB for 13 surveys collected during infiltration. Each point in Fig. 5 is an average of the change in water content for all the traces in a survey, or about 2000 data points per survey. The initial average volumetric water contents in the AB and ASB were 0.13 and 0.16, respectively, and Fig. 5 shows that the water content in both layers increased with time after infiltration. The average water content in the AB increased very steadily, with only minor fluctuations in the rate of accumulation. In contrast, the average water content in the ASB had higher fluctuations, and earlier surveys were sometimes slightly wetter than later surveys. These fluctuations may indicate temporary accumulation of water in the ASB, but they may also reflect uncertainty in the water content estimates. In the AB, which is the uppermost aggregate layer in the undrained pavement, the average water content increased by slightly less than 0.01 throughout the infiltrated period, while the average water content of the underlying ASB increased by almost 0.04. The difference in water accumulation in these layers may

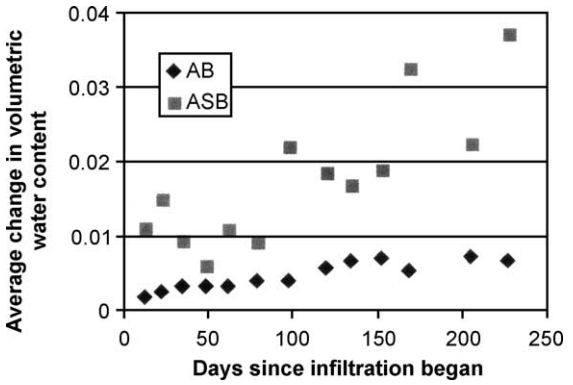

Fig. 5. Average change in water content (difference between the water content of each survey after infiltration and the water content of the initial 'dry' survey) per survey for the aggregate layers in the undrained pavement, plotted as function of time after the start of infiltration. The average changes in water content of the AB and ASB show accumulation of water with time, with greater accumulation occurring in the ASB.

indicate that water flowed more vertically, perhaps through preferential flow paths, through the lower permeability AB and then flowed more horizontally or was stored in the more permeable ASB.

Although the average water content per survey is useful for identifying trends of water accumulation or depletion, the spatial distribution of water content is more helpful for understanding possible flow patterns. To show how the spatial distribution of water content in both aggregate layers changed with time, the changes in water content along the grid of GPR traverses shown in Fig. 2a were contoured for each survey. Examples of these contour maps over the AB and ASB for the surveys collected 34, 119 and 205 days after the start of infiltration are shown in Fig. 6a–c, respectively. The dark gray or black areas on these plots indicate wetting, while the light gray or white areas indicate drying; contour lines are included to delineate wetter and dryer zones. These figures show that the water content distribution in each aggregate layer changed with time. In the AB, much of the accumulation occurred in the vicinity of the infiltration holes (at $y \approx 2.5$ m), with more pronounced areas of accumulation appearing near these holes in the later surveys. In the ASB, accumulation occurred downgradient of the infiltration holes in the earlier surveys, then spread throughout the section in later surveys. In the last surveys, the ASB showed very high water contents just downgradient of the infiltration holes, along line 2 (Fig. 2a). The ASB showed higher water contents in this area than the AB, indicating that as water flowed downgradient laterally from the infiltration holes, it also flowed vertically from the AB into the ASB. The ASB also showed areas of very high accumulation at and slightly upgradient of the infiltration holes in later surveys.

The small-scale areas of wetting and drying indicated by the GPR travel time data suggest that GPR might be used to detect localized variations in water content. This capability could be used to detect drainage between hydrological units. For example, corresponding wet areas in the aggregate layers appear to show areas of drainage from the AB into the ASB. In the survey collected 205 days after infiltration began (Fig. 6c), wet areas in the AB at (1.3, 1.5 m), (5, 2.4 m) and (5.5, 0.5 m) correspond to very wet areas in the ASB at these locations. Other areas suggest that drainage through the AB into the

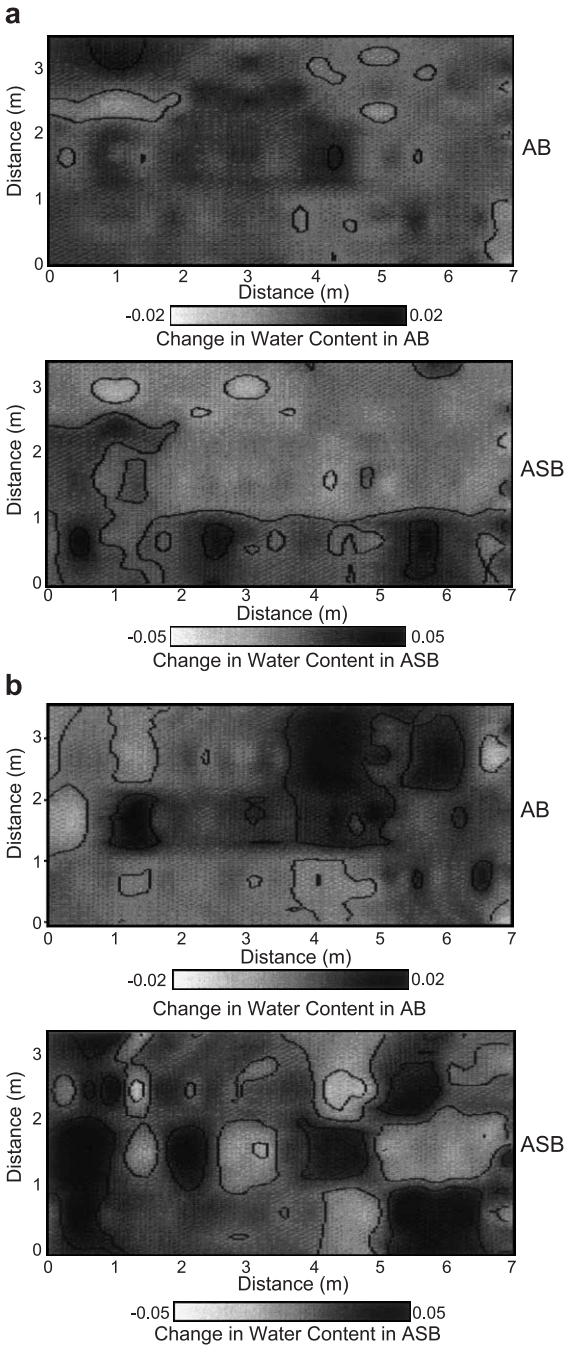

Fig. 6. Spatial distribution of the changes in water content from data collected over the undrained pavement along the GPR grid shown in Fig. 2a. The upper plot shows the changes in the water content distribution of the AB, while the lower plot shows the changes in the distribution of the ASB. (a) Survey collected at 34 days (after the start of infiltration). (b) Survey collected at 119 days. (c) Survey collected at 205 days.

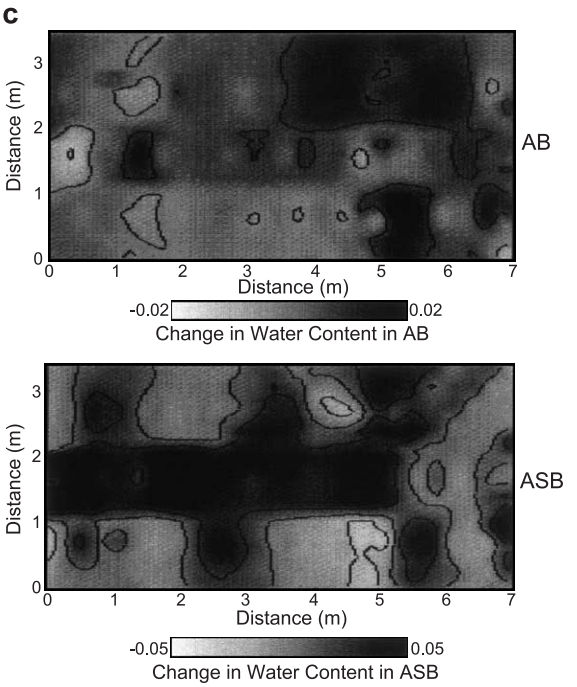

Fig. 6 (*continued*).

ASB contained some of the initial pore water as well as the introduced infiltration. An example of this occurs in each of the surveys around (0.3, 1.6 m), where a slightly dryer area in the AB corresponds to a wetter area in the ASB. Another possible zone of drainage from the AB occurs near the vertical drain located just upgradient of the section (at $y \approx 3.3$ m). In the surveys collected a few months after infiltration began, wetter areas were observed in the AB near the drain; some water may have been forced upgradient a slight distance as the downgradient section became more saturated. Similar wet zones also occurred around the drain in the ASB in later surveys, suggesting that water may have penetrated the AB and then flowed through the ASB to the vertical drain.

4.1.2. Identification of wet zones beneath the AC from GPR amplitude data

Amplitude processing and normalization were performed for the reflection from the AC–AB interface for each GPR survey to identify areas of high water content immediately beneath the AC. The changes in amplitude were calculated as the difference between the normalized amplitude at each point in a

post-infiltration survey and the normalized amplitude of that point in the 'dry' survey before the start of infiltration. Contour plots of the changes in normalized amplitude for the surveys collected 34, 119 and 205 days after the start of infiltration are given in Fig. 7. Comparison of the changes in the amplitude distribution along the AC–AB interface with the changes in the water content distribution of the AB (Fig. 6) shows that the spatial patterns of the two data sets are not very similar. Cross-plots of the change in amplitude and the change in water content for each survey confirm the lack of correlation between these parameters. The contour plots of the change in amplitude show that the amplitudes increased most near the infiltration holes (at $y \approx 2.5$ m), indicating an accumulation of water in this area. The travel time data also showed wetting near the infiltration holes, but the wet areas in the travel time data were larger and expanded to areas further from the infiltration holes with time, while the areas of high amplitude generally showed less expansion with time. The differences between the distributions of the amplitude and travel time data are probably caused by the different sampling depth of each type of measurement. The amplitude data were primarily influenced by the water content closest to the AC–AB interface (in the uppermost portion of the AB), while the travel time data were influenced by the water content across the entire thickness of the AB. Information from travel time and amplitude data might therefore be used jointly to estimate the vertical distribution of water in the AB. For example, in this experiment, the amplitude data suggest that water accumulation in the upper portion of the AB primarily occurred near the infiltration holes, while the travel time data suggest that water accumulated further from the infiltration holes in deeper portions of the AB and flowed through permeable flow paths in the AB into the ASB.

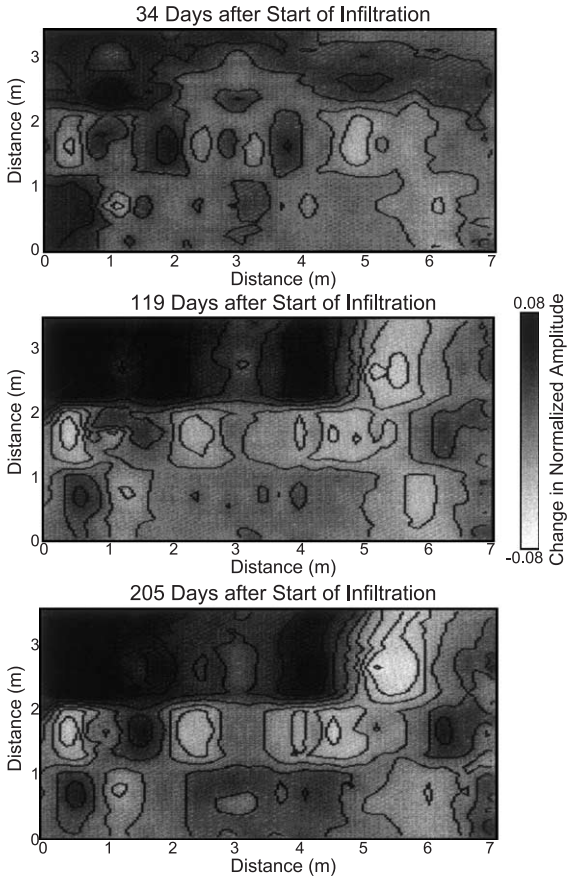

Fig. 7. Spatial distribution of the changes in normalized amplitude for the reflection from the AC–AB interface in the undrained pavement. The amplitude distributions shown here are from surveys collected 34, 119 and 205 days after the start of infiltration. Higher amplitudes are primarily observed near the infiltration holes, indicating that water is accumulating beneath the AC near these holes.

Despite the dissimilar spatial distributions of the changes in amplitude and water content for individual surveys, these parameters seem to be well correlated when the average values for each survey are considered. A cross-plot of the average change in normalized amplitude of the AC–AB reflection with the average change in water content in the AB for each survey is given in Fig. 8. This plot shows a strong positive correlation between the changes in water content and amplitude, as was expected from reflection coefficient theory (Eq. (3)). These results suggest that even though amplitude and water content were not strongly correlated for individual measurements, the volume of water accumulated near the AC–AB interface (indicated by amplitude data) was proportional to the water content throughout the AB (indicated by travel time data) for this pavement. Thus, amplitude data might be used to indicate the average water content in the aggregate layer when the accumulation near the AC–aggregate interface and the accumulation throughout the aggregate layer are correlated.

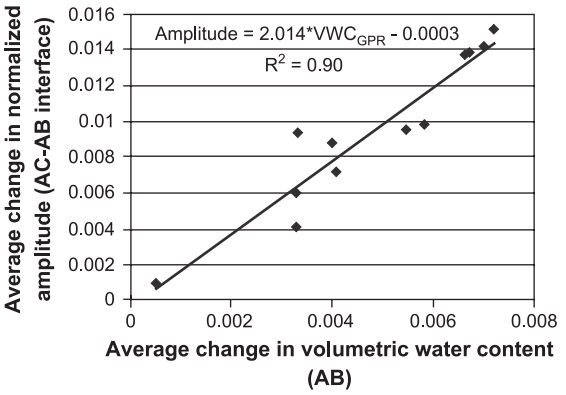

Fig. 8. Average change in normalized amplitude per survey for the reflection from the AC–AB interface in the undrained pavement, plotted as a function of the average change in water content of the AB.

4.2. Results in the drained pavement

Infiltration in the drained pavement occurred directly into the ATPB, as shown in Fig. 1b, and GPR traverses were collected along the grid indicated in Fig. 2b. Both GPR travel time and amplitude data were investigated, and the results of these analyses are discussed in Sections 4.2.1 and 4.2.2, respectively.

4.2.1. Water content estimates from GPR travel time data

The water content in each of the three aggregate layers in the drained pavement was estimated using GPR travel time data, as described in Section 3.2. Fig. 9 shows the average change in water content per survey for each aggregate layer for 12 surveys collected during infiltration. The average water contents in the AB and ASB before infiltration began were 0.12 and 0.15, respectively. The initial average water content in the ATPB was estimated as 0.06, although as discussed in Section 3.2, the accuracy of this estimate is very uncertain since no truly appropriate petrophysical relationships were available for this layer. Despite this uncertainty, the travel time data in the ATPB were converted to apparent water content values to allow comparisons between the changes in water content in the ATPB and the other aggregate layers. Fig. 9 shows that only minor fluctuations in the average water content of each aggregate layer occurred during infiltration. The lack of significant accumulation in the AB and ASB indicates that the ATPB adequately drained most of the infiltrated water, and only a very small volume of water penetrated into the underlying layers. When analyzing the trends in Fig. 9, it is important to note that in very thin layers, a small change in travel time will result in a much larger change in the estimated water content than the same change in travel time through a thicker layer. For example, the ATPB is much thinner than the other layers, so only a small change in travel time is necessary to see a significant change in the estimated water content. The fluctuations in the water content of the ATPB shown in Fig. 9 correspond to very small changes in travel time and may therefore be more prone to error than the water content fluctuations in thicker layers.

Although the average changes in the water content of the AB and ASB fluctuated between slight wetting and slight drying for different surveys, the average water contents in the ATPB showed drying immediately after the start of infiltration, then became slightly wetter with continued infiltration. A possible explanation for the drying trend observed in the ATPB is that part of the asphalt cement in the ATPB was washed out during infiltration. If the infiltrated water drained very quickly through the ATPB (as indicated by laboratory-scale permeability tests) and simultaneously removed some of the asphalt cement in the ATPB, GPR surveys collected after infiltration would show lower dielectric constants (i.e., would appear drier) than the initial survey, because the volume

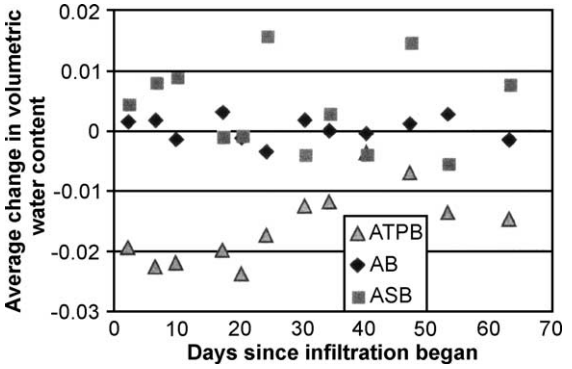

Fig. 9. Average change in water content per survey for the aggregate layers in the drained pavement, plotted as function of time after the start of infiltration. The average changes in water content of the AB and ASB fluctuate around zero, indicating no significant wetting or drying. The average changes in the water content of the ATPB show a large initial reduction in water content, then a gradual increase.

initially occupied by asphalt would then be occupied only by air. The ATPB was excavated after the infiltration experiments were concluded, and the excavation showed that a significant amount of asphalt cement had been stripped from the ATPB during infiltration. The removal of asphalt from the ATPB was probably responsible for some of the apparent drying in this layer, but because the volume of asphalt removed with time could not be measured, it was impossible to quantitatively relate the loss of asphalt to the lower dielectric constants measured in the ATPB.

Another possible explanation for the lower dielectric constants measured in the ATPB after infiltration is that a thin layer of water pooled on the low-permeability prime coat at the ATPB–AB interface, and a GPR reflection was generated from this water layer. A reflection from a thin water layer above the ATPB–AB interface has the same polarity as a reflection from the ATPB–AB interface without a water layer, and the water layer reflection arrives only slightly earlier in time than the reflection from the actual ATPB–AB interface. Even for the highest frequency (1200-MHz) GPR data used in this experiment, the wavelet resolution (pulse envelope time duration) is inadequate to distinguish between reflectors separated by less than 5.0 cm. As the thickness of the ATPB is only 7.5 cm, detecting reflections from both a water layer within the ATPB and from the interfaces defining the drainage layer (AC–ATPB and ATPB–AB interfaces) is clearly beyond the capability of the GPR equipment used in this experiment. Instead, the reflection from a thin water layer superimposes with the reflection from the ATPB–AB interface. Since the polarity of the ATPB–AB reflection and the water layer reflection are the same, and the time difference between the two reflections is small, the superposition of the two wavelets is primarily constructive. The water layer reflection arrives earlier in time than the ATPB–AB reflection, so the resulting composite (superimposed) wavelet has an earlier arrival time than the original ATPB–AB reflection. Thus, when this superimposed wavelet is chosen as the ATPB–AB interface, the ATPB appears drier.

To determine whether a thin layer of pooled water might be causing the apparent drying trend in the ATPB, two additional experiments were performed. In the first experiment, a short-term infiltration test was performed on an adjacent pavement section, where a very large volume of water was rapidly infiltrated into the ATPB during GPR data collection. The GPR data showed very small travel times in the ATPB (a reduction in water content) immediately downgradient of the infiltration zone, indicating that a reflection was generated from the pooled water in this area. To quantify how the depth of pooled water affected the reflection from the ATPB–AB interface, a second, laboratory-scale experiment was performed with a small block (52 by 41 cm) of AC and ATPB placed in a plastic tub. Water was gradually added to the tub and GPR surveys were collected across the block after each addition of water. Data for the block experiment was interpreted and the average apparent water content for each survey was estimated using the same techniques as for the field-scale experiments. (Since the water content estimates in the block experiment are known to be erroneous due to the reflection from the water layer, these estimates will be referred to as the ‘apparent’ water content.) Fig. 10 shows the average change in the apparent water content of the ATPB for each survey in the block experiment plotted as a function of the depth of the water layer in the ATPB. These results clearly show that pooled water could cause the ATPB to appear to be very dry, with the lowest water contents corresponding to the great-

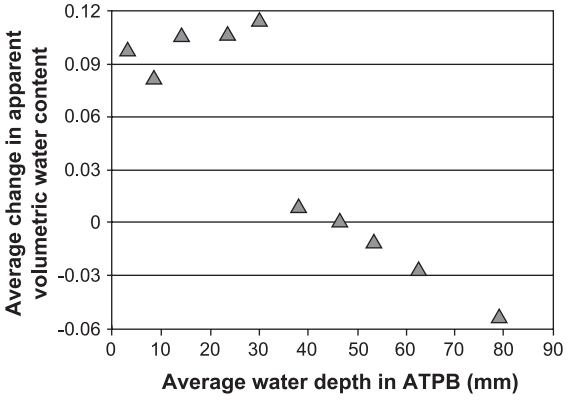

Fig. 10. Average change in apparent water content per survey in the ATPB for the laboratory-scale block experiment, plotted as a function of the water depth in the ATPB. When the water was less than ~3 cm deep, the changes in water content show significant wetting. When the water was deeper than ~5 cm, the changes indicate drying.

est depths of pooled water, when the water layer was thick enough (greater than ~3.5 cm) to generate a reflection. However, when the depth of the pooled water was small, the ATPB appeared wetter, as the travel time through the ATPB was increased even though the water layer was too thin to generate a reflection. For thicker water layers in the ATPB, the reflection from the AC–ATPB interface became harder to identify due to destructive superposition with the water layer reflection; this destructive superposition may explain some of the difficulty in clearly identifying the AC–ATPB reflection in later surveys in the large-scale experiments.

Although the GPR data in the block experiment appropriately indicated wetting for very thin layers of pooled water, these measurements did not accurately estimate the water content in the ATPB; the errors are likely due to wavelet superposition and to the inappropriate application of Topp's equation in a non-homogenous media. Thus, GPR travel time data through the ATPB cannot be used to reliably estimate the water content in the ATPB under conditions of very high infiltration. Despite the limitations of GPR data for estimating water content in the ATPB during rapid infiltration, GPR data can still be used to indicate wetter and drier areas in this layer under normal infiltration conditions in pavements with slopes sufficient to drain the ATPB.

To observe how water content fluctuated spatially in the drained pavement, contour maps were generated of the changes in water content in the ATPB, AB and ASB using GPR data acquired along the grid shown in Fig. 2b. Examples of these contour maps for the surveys collected 2, 30 and 63 days after the start of infiltration are shown in Fig. 11a–c, respectively. These plots show that although the average water content per survey does not change significantly with time, considerable spatial variations occur within each survey. Accumulation of water consistently occurs around (6, 0.75 m) in the ATPB and around (3.5, 0.5 m) in the ASB, while depletion occurs around (1.5, 1.5 m) in the ATPB. As in the undrained pavement, corresponding areas of accumulation in the aggregate layers appear to show areas of drainage between layers. For example, the wetter zone in the AB around (0.5, 3 m) corresponds to a slightly wetter zone at the same location in the ASB and may indicate a flow path between these layers.

Although the spatial variations in water content for each survey were sometimes considerable, there was only a moderate redistribution of water within each layer with time. This relatively static water content distribution suggests that the small volume of water that penetrated into the AB and ASB tended to repeatedly infiltrate along preferential flow paths rather than spreading throughout the layer. Areas where the prime coat of sprayed asphalt did not penetrate well or an inadequate amount of prime coat was applied would be likely areas where water could infiltrate from the ATPB into the AB. Time-lapse GPR surveys of each of the aggregate layers, as acquired in this experiment, may help to identify these areas.

4.2.2. Identification of wet zones beneath the AC from GPR amplitude data

The amplitudes of the reflection from the AC–ATPB interface were processed and normalized by the airwave amplitudes, and the changes in amplitude (compared to the initial 'dry' survey) were calculated for each survey. Contour plots of the change in normalized amplitude are shown in Fig. 12 for the surveys collected 2, 30 and 63 days after the start of infiltration. Comparison of these plots with the changes in water content of the ATPB calculated from travel time data (Fig. 11) shows that there is no obvious spatial correlation between the amplitude and water content estimates, although some consistently wetter areas appear to have higher amplitudes. Cross-plots of the changes in amplitude and water content at each point were also generated for each survey, and as with the undrained pavement, these plots again showed no significant correlation between amplitude and water content within a single survey. Fig. 13 shows the average change in normalized amplitude for the AC–ATPB reflection plotted against the corresponding average change in water content of the ATPB for each survey. This plot shows a weak trend of higher amplitudes corresponding to lower water contents, but the scatter in the data is too large to meaningfully relate amplitude data to water content estimates.

To clarify the relationship between amplitude and water content for the drained pavement, amplitude analysis was also performed on the data from the short-term, high-volume infiltration experiment conducted in an adjacent drained pavement section. The results of

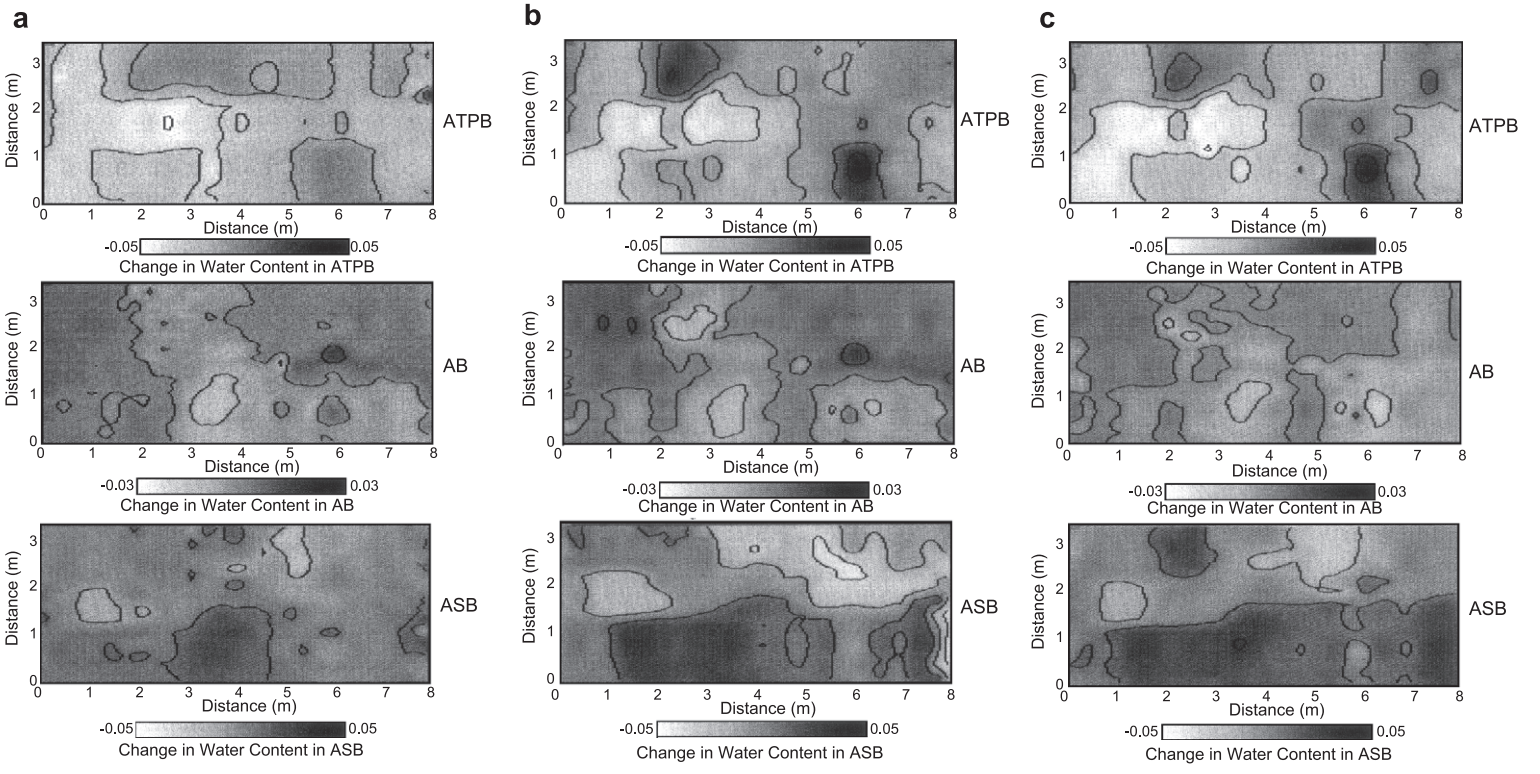

Fig. 11. Spatial distribution of the changes in water content from data collected over the drained pavement along the GPR grid shown in Fig. 2b. The uppermost plot shows the changes in the water content distribution of the ATPB, the middle plot shows the changes in the distribution of the AB, and the lowermost plot shows the changes in the distribution of the ASB. (a) Survey collected at 2 days (after the start of infiltration). (b) Survey collected 30 at days. (c) Survey collected at 63 days.

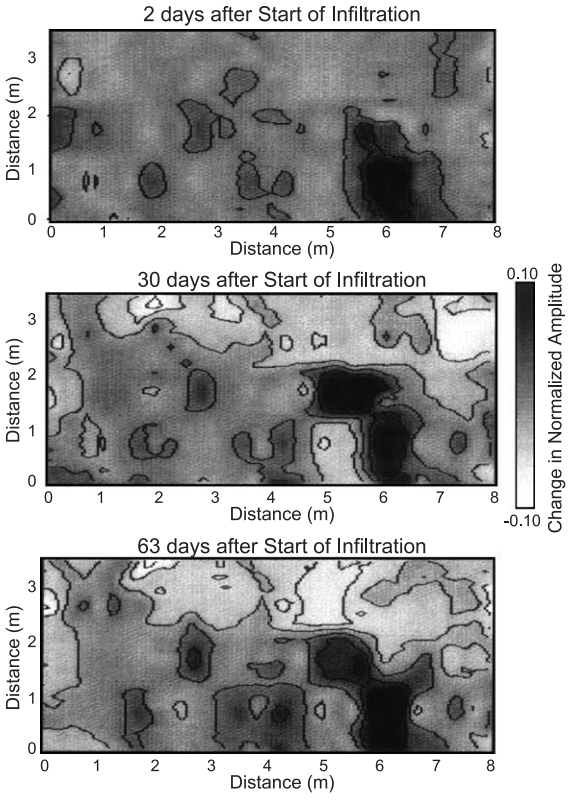

Fig. 12. Spatial distribution of the changes in normalized amplitude for the reflection from the AC–ATPB interface in the drained pavement section. The amplitude distributions shown here are from surveys collected 2, 30 and 63 days after the start of infiltration.

this analysis indicate that the average changes in amplitude and water content are strongly correlated, as shown in Fig. 13. However, this experiment showed that the largest changes in amplitude are correlated to the greatest reductions in water content, which is opposite the trend expected from reflection coefficient theory. These results are due to the influence of pooled water in the ATPB, which causes a very large change in the reflection amplitude, but also causes the travel time measurements to indicate very 'dry' water contents (Section 4.2.1). Thus, high amplitudes correspond to areas of pooled water, as was observed in amplitude contour plots for the short-term infiltration experiment. Amplitude data may therefore be used in conjunction with travel time measurements to determine whether areas that are indicated as 'dry' in the travel time data correspond to actual drying or to areas of pooled water.

4.3. Validation of the water content estimation procedure and discussion of errors

After the infiltration experiment in each pavement section was completed, a final GPR survey was performed over selected locations in the GPR grid, for a total of 11 locations in the 2 sections. For the drained pavement, GPR data were collected in a single traverse across the selected locations; for the untrained pavement (collected later), data were collected in two perpendicular traverses that intersected over the selected location. For both sections, the AC was cored immediately after the GPR surveys at the selected locations using a dry-bit drilling technique, and gravimetric water content measurements were collected in the AB and ASB. The gravimetric measurements were collected in continuous vertical increments of 2–3 cm and were converted to volumetric water content estimates using the average density of each layer, as determined from pavement construction records. These estimates were then arithmetically averaged for each aggregate layer for comparison with the GPR-derived water content estimates. In general, the GPR-derived estimates of water content in the aggregate layers were quite accurate, with a root mean squared error of 0.021 $cm^3/$

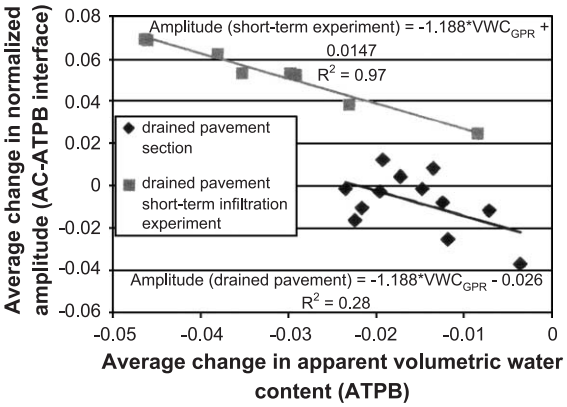

Fig. 13. Average change in the normalized amplitude per survey for the reflection from the AC–ATPB interface in the drained pavement section and in the adjacent (drained) pavement section with short-term infiltration, plotted as a function of the average change in apparent water content of the ATPB. The changes in amplitude from the drained pavement section show little correlation with the changes in water content, but the changes in amplitude from the short-term infiltration experiment in the adjacent drained pavement are highly correlated with the changes in water content.

cm^3. Fig. 14 shows a plot of the water content estimates from GPR data and from gravimetric water content measurements. In this plot, two estimates are shown for each borehole drilled in the drained section (one AB estimate and one ASB estimate). For the undrained pavement, two GPR traverses were collected over each location, so two estimates are shown for the AB and two are shown for the ASB.

Fig. 14 shows that the water content estimates from GPR and gravimetric measurements have reasonably good correlation but, the scatter in the data is not negligible. The differences between the GPR and gravimetric measurements may be caused by several different factors, including inaccurate estimates of the pavement aggregate properties, errors in the interpretation and processing of the GPR data, and differences in the water volumes measured with gravimetric or electromagnetic techniques.

Accurate characterization of the pavement aggregates is necessary to obtain precise volumetric water content estimates from either GPR or gravimetric techniques. For GPR techniques, the pavement thickness is used to convert the GPR travel time measurements to water content, so variations in the thickness of the aggregate layers cause error in the GPR water content estimates. Slight variations in the thickness of the aggregate layers seem probable in these pavement sections, as the GPR surveys collected before the start of infiltration indicated that the thickness across each layer was not perfectly uniform. For example, the traverses shown in Figs. 3 and 4 were collected before infiltration began in the undrained and drained pavement sections, respectively, and the travel time measurements for each layer changed somewhat across each section. If gravimetric techniques are used to estimate water content, the pavement thickness is not required, but an estimate of the soil density is needed to convert the gravimetric water content measurements to volumetric water content estimates. Inaccurate soil density estimates or variations in density throughout an aggregate layer may produce inaccurate volumetric water content estimates.

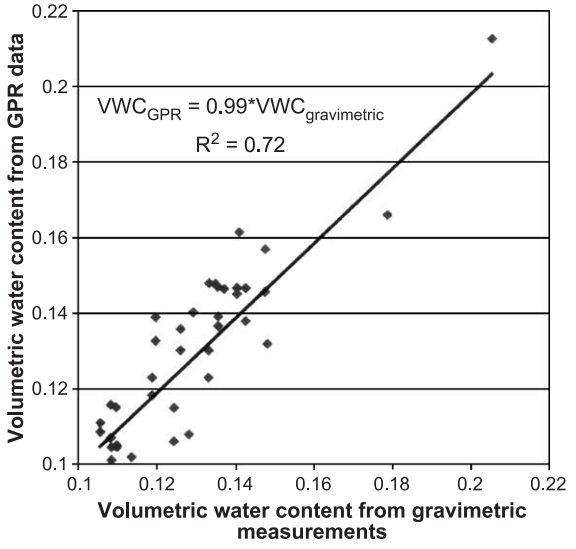

Fig. 14. Comparison of volumetric water content estimates derived from GPR data and from gravimetric sampling.

Uncertainties in the interpretation and processing of the GPR data may also contribute to the error in the GPR-derived water content estimates. One source of uncertainty is the use of data with different central frequencies to calculate the travel time through the ASB. Since data from different frequency antennas have slightly different travel paths (contributing to slightly different arrival times) and different resolutions, merging data sets with different central frequencies can complicate data interpretation and introduce errors in travel time measurements. Another error introduced by using multi-frequency data sets is that the airwave cannot be chosen with complete accuracy for each frequency, and the airwave is used to define the zero time for both data sets. In Figs. 3 and 4, the airwave 'pick' in the 900-MHz data appears to be fairly free from superposition with the groundwave, but CMP surveys could not be collected for the 1200-MHz antenna, so it is not clear how much, if any, superposition occurs between the airwave and groundwave for the 1200-MHz data. Also, superposition of the airwave and groundwave may occur for either frequency if the properties of the surface layer (the AC) change at locations further from the CMP survey. For this experiment, errors in the zero time estimation caused, by airwave and groundwave superposition should affect only the travel time measurements in the ASB, as this is the only layer for which data from both frequencies are used. Comparison of errors in the water content estimates for the AB and ASB show that the ASB estimates are on average slightly more accurate than the AB estimates, suggesting that error introduced by merging data sets of different frequencies is not

more significant than the other sources of error discussed here.

Another potential source of error in the GPR data collected in this experiment is wavelet superposition, which can obscure the exact arrival time of different reflections. For this experiment, superposition was most significant for the reflection from the AC–ATPB interface. For the 1200-MHz data, this reflection could be identified fairly easily in the early (drier) surveys, although it had a low amplitude and was probably partially superimposed with the leading edges of the reflection wavelet from the ATPB–AB interface. In later surveys, the amplitude of the AC–ATPB reflection was further reduced and occasionally had polarity reversals; the change in this reflection is most likely caused by increased wavelet superposition due to reflections from pooled water. In the 900-MHz data, the reflections from the AC–ATPB and ATPB–AB interfaces were merged into a single reflection, so the reflection from the AC–ATPB interface could not be identified in any survey. The superposition of these two reflections also prevented accurate measurement of the arrival time of the ATPB–AB reflection, thus eliminating the possibility of accurately measuring the travel time through the AB using only 900-MHz data.

Although errors may occur in the estimation of volumetric water content with either GPR or gravimetric techniques, the water contents estimated with these techniques may also differ as a function of the volume of water measured with each method. Gravimetric techniques measure the entire volume of water in a sample, including water held to the soil surface by electromolecular forces (bound water) and water free to move in the soil pores (free water). In contrast, GPR techniques primarily measure free water and are less sensitive to bound water, which cannot rotate as freely in the presence of an applied electromagnetic field (Boyarskii et al., 2002; Serbin and Or, 2003). Thus, if a significant portion of the water in a soil is bound, the water content estimated with gravimetric techniques should be greater than the water content estimated with GPR techniques. In this experiment, the water content estimates from gravimetric techniques were on average only slightly higher (difference in volumetric water content of 0.001) than the estimates from GPR techniques, indicating that the differences between the GPR and gravimetric estimates of water content were not greatly influenced by bound water effects.

5. Summary and conclusions

These experiments have shown that ground-coupled GPR techniques can be used to estimate the volumetric water content in sub-asphalt aggregate layers with high resolution, in multiple dimensions, and in a non-invasive manner. The GPR-derived estimates of water content calculated in these experiments had relatively low errors (RMSE of 0.021 cm^3/cm^3), suggesting that this technique has potential for use in routine pavement surveys when the average thickness of the aggregate layer was recorded during construction and the actual thickness of the aggregate layer is usually similar to the average thickness. Although this technique seemed to work well for this experiment, some changes in the procedures might make it more practical for large-scale surveying. One change that would greatly simplify data collection and processing would be to use a single, lower-frequency antenna instead of multi-frequency data, if a slight reduction in accuracy is acceptable. Higher frequency GPR data provide better resolution and thus more accurate water content estimates than lower frequency data, but may not have the depth penetration needed to image the deepest reflector. Lower frequency data can provide better depth penetration and may allow adequate penetration from an air-launched antenna, thus reducing the time needed to collect data. Using data from one frequency also reduces uncertainty in the data interpretation and processing routine. However, the circumstances in which lower frequency data are appropriate must be analyzed for each pavement; in pavements with thin aggregate layers (such as a drainage layer), using lower frequency data that cannot accurately image reflections near the thin layer may produce unacceptably large errors.

The results of this experiment provided information on how water may infiltrate pavement aggregates. Analysis of the water content estimates calculated from GPR travel time data in both pavement sections indicates that the sub-asphalt drainage layer is effective, as significant wetting of the aggregate layers occurred in the undrained pavement, but not in the drained pavement. Within the drainage layer,

analysis of the travel time data sometimes indicated drying after infiltration; this apparent drying may signify areas of pooled water, which can be more accurately identified using both amplitude and travel time data. Apparent drying in the drainage layer may also denote stripping of the asphalt cement in this layer, but further research is needed to quantitatively verify this hypothesis.

GPR travel time data were also useful for indicating the spatial distribution of water within the aggregate layers. In the AB, water appeared to flow primarily through localized zones of high water content, while the water content increased more uniformly across the section in the ASB (for the undrained pavement). This spatial distribution might indicate piping or preferential flow paths through the AB and more distributed flow through the deeper ASB. Analysis of the water content distribution in the aggregate layers may be useful for detecting leaks through the prime coat and indicating areas of localized piping.

Joint analysis of travel time and amplitude data showed that the reflection amplitude for the interface between the AC and the first aggregate layer has potential for indicating the water content in this aggregate layer for some undrained pavements. Knowledge of the water content near the asphalt–aggregate interface could also be used to predict asphalt stripping and deterioration. Although the data in this study were collected using ground-coupled GPR, amplitude analysis of the AC–aggregate reflection could also be performed using the more commonly acquired air-launched GPR data. With air-launched data, the thickness of the AC could be measured using conventional reflection coefficient and travel time analyses, and areas of high water content beneath the AC could be identified by analyzing the amplitudes of the AC–aggregate reflection. The results of the amplitude and travel time analyses in this study also have important implications for the application of GPR reflection coefficient techniques to estimate the thickness of aggregate layers. Using reflection coefficient theory, amplitudes from the AC–aggregate reflection may be used to determine the dielectric constant of the aggregate layer, and the dielectric constant is then employed in conjunction with travel time measurements to estimate the layer thickness. This study has shown that reflection amplitudes may not be strongly correlated to the average dielectric constant of the underlying layer; substantial errors in the thickness estimates may occur if the dielectric constant immediately adjacent to the interface differs significantly from the dielectric constant throughout the aggregate layer. Other errors in the thickness estimates could be caused by inaccurate dielectric constant estimation due to conditions such as pooled water in drained pavements.

The results of this experiment have shown that GPR data can be used to monitor the water content in sub-asphalt aggregate layers. For very accurate water content estimates, the thickness of each aggregate layer must be well characterized, but reasonably good estimates were obtained using the average thickness of each layer recorded during pavement construction. The water content estimates can be mapped to show the water content distribution in each layer and to indicate the locations of preferential flow paths between layers. Water content estimates obtained from GPR data can contribute to more efficient pavement maintenance and rehabilitation by identifying areas of poorly drained aggregates, determining the efficacy of the sub-asphalt drainage layer and detecting areas of likely asphalt deterioration.

Acknowledgements

This study was funded by Caltrans through the Partnered Pavement Research Center and NSF EAR-0087802 to Prof. Yoram Rubin and Prof. John Harvey. We sincerely thank Prof. Michael Riemer (Dept. of Civil and Env. Eng., Univ. of California, Berkeley) for his unfailing support and advice throughout the experiment, Dr. Michael Herkelrath (USGS, Menlo Park) for providing the laboratory data to create petrophysical relationships, and Ed Diaz and staff (Richmond Field Station, Univ. of California, Berkeley) for their assistance with data collection. We also wish to thank Dr. A. Hördt, Dr. Neil Anderson and Dr. Timo Saarenketo for their insightful reviews of this manuscript; we feel that their suggestions have significantly improved the presentation of this research. The GPR processing was carried out at the Center for Computational Seismology (CCS) at Lawrence Berkeley National Laboratory.

References

Alharthi, A., Lange, J., 1987. Soil water saturation: dielectric determination. Water Resour. Res., 32, 591–595.

Bomar, L.C., Horne, W.F., Brown, D.R., Smart, J.L., 1988. Determining deteriorated areas in Portland cement concrete pavements using radar and video imaging. NCHRP, vol. 304. Transp. Res. Board, Washington, DC.

Boyarskii, D.A., Tikhonov, V.V., Komarova, N.Y., 2002. Model of dielectric constant of bound water in soil for applications of microwave remote sensing. Prog. Electromagn. Res., 35, 251–269.

Clemena, G., 1983. Nondestructive inspection of overlaid bridge decks with ground-penetrating radar. Transp. Res. Rec., vol. 899. Transp. Res. Board, Washington, DC.

Clemena, G., Sprinkel, M., Long, R., 1986. Use of ground penetrating radar for detecting voids underneath a jointed concrete pavement. Final Rep. Virginia Hwy. and Transp. Council, Charlottesville, VA.

Cuvillier, M., Boaddard, J.F., Retour, P., 1987. New methods developed in France for road network survey and maintenance. Proc. 6th Conf. Struct. Des. of Asphalt Pavements, vol. 1. Univ. of Michigan, Ann Arbor, MI.

Davis, J.L., Annan, A.P., 1977. Electromagnetic detection of soil water content: progress report 1. Can. J. Remote Sens., 1 (3), 76–86.

Davis, J.L., Annan, A.P., 1989. Ground-penetrating radar for high-resolution mapping of soil and rock stratigraphy. Geophys. Prospect., 37, 531–551.

Du, S., Rummel, P., 1994. Reconnaissance studies of moisture in the subsurface with GPR. GPR 94, Proc. 5th Intl. Conf. on GPR, Kitchener, Ontario, vol. 3, pp. 1241–1248.

Eckrose, R., 1989. Ground penetrating radar supplements deflection testing to improve airport pavement evaluations. In: Bush III, A.J., Daladi, G.Y. (Eds.), Non-destructive Testing of Pavements and Back Calculation of Moduli, ASTM Spec. Tech. Publ., Philadelphia, PA, vol. 1026.

Fang, H.-Y., 1991. Foundation Engineering Handbook. Van Nostrand Reinhold, New York.

Fernando, E., Maser, K.R., 1991. Development of a procedure for automated collection of flexible pavement layer thicknesses and materials: phase 1. Demonstration of existing ground penetrating radar technology. Phase 1 Final Report, Florida DOT, Tallahassee, Fla.

Greaves, R.J., Lesmes, D.P., Lee, J.M., Toksoz, M.N., 1996. Velocity variations and water content estimated from multi-offset ground penetrating radar. Geophysics, 61, 683–695.

Grote, K., Hubbard, S., Rubin, Y., 2002. GPR monitoring of volumetric water content in soils applied to highway construction and maintenance. Lead. Edge Explor., 21 (5), 482–485.

Grote, K., Hubbard, S., Rubin, Y., 2003. Field-scale estimation of volumetric water content using GPR groundwave techniques. Water Resour. Res., 39 (11), SBH5-1–SBH5-11.

Heath, A., 2002. Modeling unsaturated granular pavement materials using bounding surface plasticity. Ph.D. dissertation, University of California, Berkeley.

Hicks, R.G., 1970. Factors influencing the resilient properties of granular materials. Ph.D. dissertation, University of California, Berkeley.

Hubbard, S., Grote, K., Rubin, Y., 2002. Estimation of near-subsurface water content using high frequency GPR ground wave. Leading Edge of Exploration, vol. 21 (6). Society of Exploration Geophysics, pp. 552–559.

Hubbard, S.S, Zhang, J., Peterson, J.E., Monteiro, P.J.M., Rubin, Y., 2003. Non-invasive rebar corrosion detection using geophysical methods. ACI Mater. J., 100 (2), 501–510.

Kelley, E.J., 1999. Soil moisture effects in pavement systems. M.S. thesis, Ohio University, Athens.

Lesmes, D., Herbstzuber, R.J., Wertz, D., 1999. Terrain permittivity mapping: GPR measurements of near-surface soil moisture. Proc. SAGEEP, Environmental and Engineering Geophysical Society, pp. 575–582.

Lunt, I., Hubbard, S., Rubin, Y., 2003. Estimation of soil water content using ground penetrating radar reflection travel time data. Submitted to. J. Hydrol., accepted.

Maser, K.R., 1991. Bridge deck condition surveys using radar: case studies of 28 New England decks. Transp. Res. Rec., vol. 1304. Transp. Res. Board, Washington, DC.

Maser, K.R., 1996. Condition assessment of transportation infrastructure using ground-penetrating radar. J. Infrastruct. Syst., 2 (2), 94–101.

Maser, K.R., Rawson, A., 1992. Network bridge decks surveys using high speed radar; case studies of 44 decks. Transp. Res. Rec., vol. 1347. Transp. Res. Board, Washington, DC.

Narayanan, R.M., Hudson, S.G., Kumke, C.J., 1998. Detection of rebar corrosion in bridge decks using statistical variance of radar reflected pulses. GPR 98, Proc. 7th Intl. Conf. on GPR, Lawrence , Kansas, vol. 2, pp. 601–605.

Roddis, W.M.K., Maser, K.R., Gisi, A.J., 1992. Radar pavement thickness evaluations for varying road base conditions. Transp. Res. Rec., vol. 1355. Transp. Res. Board, Washington, DC.

Roth, K., Schulin, R., Fluhler, H., Attinger, W., 1990. Calibration of time domain reflectometry for water content using a composite dielectric approach. Water Resour. Res., 26 (10), 2267–2273.

Saarenketo, T., Scullion, T., 1994. Ground penetrating radar applications on roads and highways. Res. Rep., vol. 1923-2F. Texas Transp. Inst., College Station, TX.

Saarenketo, T., Scullion, T., 2000. Road evaluation with ground penetrating radar. J. Appl. Geophys., 43, 119–138.

Saarenketo, T., Nikkinen, T., Lotvonen, S., 1994. The use of ground penetrating radar for monitoring water movement in road structures. Proc. 5th Intl. Conf. on GPR, June 12–16, Kitchener, Ontario, vol. 3 of 3, pp. 1181–1192.

Scullion, T., Rmeili, E., 1997. Detecting Stripping in Asphalt Concrete Layers Using Ground-penetrating Radar. Texas DOTPD Rep. TX-97-2964-S, Austin, TX.

Scullion, T., Lau, C.L., Chen, Y., 1994. Pavement evaluations using ground penetrating radar in Texas. Proc. 5th Intl. Conf. on GPR, June 12–16, Kitchener, Ontario, vol. 1 of 3, pp. 449–463.

Scullion, T., Chen, Y., Lau, C.L., 1995. Colormap—user's Manual with Case Studies. Texas DOTPD Rep. TX-95-1341-1, Austin, TX.

Serbin, G., Or, D., 2003. Near-surface soil water content measurements using horn antenna radar: methodology and overview. Vadose Zone J., 2, 500–510.

Smith, S., Scullion, T., 1993. Development of ground-penetrating radar equipment for detecting pavement condition for preventive maintenance. Final Rep., Strategic Hwy. Res. Program, Project H-104 A, Nat. Res. Council, Washington, D.C.

Topp, G.C., Davis, J.L., Annan, A.P., 1980. Electromagnetic determination of soil water content: measurements in coaxial transmission lines. Water Resour. Res., 16 (3), 574–582.

Ulriksen, C.P.F., 1992. Application of impulse radar to civil engineering. Ph.D. Thesis, Dept. of Engineering Geology, Lund University of Technology, Sweden.

Van Overmeeren, R., Sariowan, S., Gehrels, J., 1997. Ground penetrating radar for determining volumetric soil water content; results of comparative measurements at two test sites. J. Hydrol., 197, 316–338.

Weiler, K.W., Steenhuis, T.S., Bull, J., Kung, K.-J.S., 1998. Comparison of ground penetrating radar and time domain reflectometry as soil water sensors. Soil Sci. Soc. Am. J., 62, 1237–1239.